LETTER

ACS chemical biology

Mechanism of an Amphipathic α-Helical Peptide's Antiviral Activity Involves Size-Dependent Virus Particle Lysis

Nam-Joon Cho[†], Hadas Dvory-Sobol[†], Anming Xiong[†], Sang-Joon Cho[∥], Curtis W. Frank[§], and Jeffrey S. Glenn[†,‡,*]

[†]Department of Medicine, Division of Gastroenterology and Hepatology, Stanford University School of Medicine, [‡]Palo Alto Veterans Administration, [§]Department of Chemical Engineering, Stanford University, Stanford, California 94305, and [∥]Park Systems Corp., Suwon, Korea

End-stage liver disease (ESLD) is a major cause of worldwide morbidity and mortality. Viral infections, such as those resulting from the hepatitis C virus (HCV), are important etiologies. Current interferon-based therapies for HCV are inadequate for most patients; hence, a great need to develop and evaluate new potential antiviral strategies exists (*1*). Disrupting NS5A membrane association represents a new, attractive anti-HCV strategy because the protein has been genetically validated as essential for HCV RNA genome replication (*2, 3*). While studying the NS5A-derived AH peptide's binding interaction with cell-derived and model membranes (*3–5*), we discovered a surprising property of the AH peptide: its ability to induce lysis of lipid vesicles as well as virus particles, thereby inhibiting *de novo* HCV infection. Dynamic light scattering (DLS) was employed to study the vesicle size dependency of AH peptide-mediated vesicle lysis as a model system for virus particle lysis. From these studies, we identified a vesicle size range within which the AH peptide shows vesicle lysis potency. To further examine this lysis activity, we investigated how vesicle size affects the AH peptide's vesicle rupturing ability in order to better understand the mechanism of virus particle lysis. Previously, we described a novel method that employs the AH peptide to destabilize a layer of intact vesicles adsorbed on various substrates such as gold and titanium oxide. The AH peptide interaction causes vesicle rupture, transforming the adsorbed vesicles into a planar bilayer (*5*). We used the quartz crystal microbalance-dissipation (QCM-D) technique as a detection system with nanoscale mass range precision to measure the degree of vesicle rupture (*6*). This technique not only measures the quantitative binding mass that can be derived from the simple linear relationship, the Sauerbrey equation, between the crystal's resonant frequency change and the mass of the adlayer (*7*), but the viscoelasticity of the adlayer, providing insight into peptide conformational changes upon binding, can also be deduced by the damping of the crystal oscillation (*6*).

The vesicle size range of the AH peptide's vesicle rupturing ability was in good agreement with the vesicle size range of the AH peptide's lysis activity, suggesting that these two platforms, modeling virus particles adsorbed to a solid substrates and in bulk solution, are appropriate and complementary tools to investigate the AH peptide's antiviral activity. Atomic force microscopy (AFM) studies revealed additional insight into the AH peptide's mode of action with model virus particles. Based on the virus particle size range identified with the model system that corresponds to AH peptide's proposed lysis potency, infectivity assays were performed and confirmed that AH peptide is able to inhibit the activity of a virus particle within this size range. For the first time, a correlation between virus

ABSTRACT The N-terminal region of the hepatitis C virus (HCV) nonstructural protein NS5A contains an amphipathic α-helix that is necessary and sufficient for NS5A membrane association. A synthetic peptide (AH) comprising this amphipathic helix is able to lyse lipid vesicles that serve as a model system for virus particles. Based on quartz crystal microbalance-dissipation (QCM-D) experiments, the degree of vesicle rupturing was found to be inversely related to vesicle size, with maximal activity in the size range of several medically important viruses. In order to confirm and further study vesicle rupture, dynamic light scattering (DLS) and atomic force microscopy (AFM) experiments were also performed. The size dependence of vesicle rupturing helps explain the peptide's observed effect on the infectivity of a wide range of viruses. Further, *in vitro* studies demonstrated that AH peptide treatment significantly decreased the infectivity of HCV particles. Thus, the AH peptide might be used to rupture HCV particles extra-corporally (for HCV prevention) and within infected individuals (for HCV therapy).

*Corresponding author, jeffrey.glenn@stanford.edu

Received for review June 30, 2009 and accepted November 24, 2009.

Published online November 24, 2009

10.1021/cb900149b CCC: $40.75

particle size and AH peptide's lysis potency has been discovered, revealing key insights into the mechanism of the hepatitis C virus NS5A AH peptide's antiviral activity.

We first confirmed the α-helical character of the AH peptide with the circular dichroism (CD) technique, as shown in Figure 1. The blue spectrum (AH peptide) displays two peaks at 209 and 222 nm, corresponding to α-helical secondary structure. The AH peptide is mostly a helix (>85%), which is also illustrated in the helix net diagram (Figure 1, panel a). The amphipathic nature of the helix (indicated by the blue band in the helix net diagram) is conserved across all natural HCV isolates (*2*). A control NH peptide, in which three point mutations were introduced into the AH peptide in order to disrupt its hydrophobic face, was also studied. These mutations consisted of three charged amino acids (indicated as the bold, underlined residues presented in Methods) spaced at specific intervals along the AH peptide's predicted α-helix such that no sustained hydrophobic patch remained (Figure 1, panel b). The NH peptide is clearly distinguished in the red spectrum (Figure 1, panel c) as mainly possessing a random coil structure (>80%) with little helical character (<20%).

To further investigate the AH peptide's lysis potency (*5*), with respect to the size dependency of the target vesicles, we employed the DLS technique, which measures the changes in the average size and relative variance (polydispersity) of vesicles in solution upon addition of the AH peptide. The series of size distribution changes after adding the AH peptide, as well as control experiments including NH peptide addition and no peptide addition, as a function of time are presented in Figure 2, panels a−c. First, we measured the initial vesicle size distribution, which corresponded to an intensity-weighted average diameter, D_a, of 58.4 ± 0.2 nm and polydispersity, Δ_2, of 0.064 ± 0.006 (Figure 2, panel a). Upon addition of the AH peptide, we then measured the vesicle size and polydispersity changes over the next 30 min. As shown in Figure 2, panel b, the average diameter and polydispersity changed to 135.3 ± 2.5 nm and 0.134 ± 0.056, respectively, as a result of the presumed membrane disruption and reassembly of the vesicles. Addition of the NH peptide control had no such effect on the vesicles (Figure 2, panel c). In contrast, however, the addition of AH peptide to larger vesicles with an average diameter of 299.3 ± 8.4 nm with a polydispersity of 0.301 ± 0.046 altered neither the size nor the polydispersity of the vesicles (Supplementary Figure S1), presumably due to the vesicles' insufficient line tension for AH peptide-mediated vesicle lysis.

To further understand the vesicle size dependency of the AH peptide's lysis potency, we constructed an intact vesicle platform on a gold substrate from vesicles of varying average diameters. Because of the additional factor of vesicle−substrate interactions, the intact vesicle platform permits us to better quantify the AH peptide's lysis potency by examining its rupturing ability of substrate-adsorbed, intact vesicles. QCM-D measurements indicated that the AH peptide's lysis potency has three distinct regimes related to (i) complete vesicle rupture and bilayer formation for vesicles with average diameters ranging from 59 to 67 nm (Figure 3, panels a and b, black and red traces), (ii) incomplete vesicle rupture and bilayer formation for vesicles with an average diameter greater than 90 nm (Figure 3, panels a and b, green trace), and (iii) no vesicle rupture or bilayer formation for significantly larger vesicles (Figures 3, panels c and d). For complete bilayer formation as described in regime (i), the QCM-D frequency and dissipation responses reached final values characteristic of bilayers of −26 Hz and 0.08×10^{-6}, respectively. The incomplete bilayer formation of regime (ii) is evidenced by only small decreases in the QCM-D frequency and dissipation responses to final values of −125 ± 12 Hz and 23×10^{-6}, respectively. In the case of much larger vesicles with average diameters greater than 200 nm, the AH peptide lysis potency decreased to such a degree that the QCM-D frequency and dissipation responses, as seen in regime (iii), indicate that AH peptide binding to the vesicle platform is the predominant interaction rather than vesicle rupture and bilayer formation (Figure 3, panels c and d).

The degree of vesicle rupturing was quantified to further investigate regimes (i) and (ii). Based on the initial frequency change associated with the adsorbed, intact vesicle layer ($\Delta F_{platform}$) and the final frequency value following AH peptide interaction (ΔF_{final}), we calculated the rupturing percentage (Figure 3, panel e) by the following equation:

$$\text{rupturing (\%)} \cong 1 - \frac{\Delta F_{final} - \Delta F_{bilayer}}{\Delta F_{platform} - \Delta F_{bilayer}} \times 100 \quad (1)$$

where $\Delta F_{platform}$ and ΔF_{final} are described above, and $\Delta F_{bilayer}$ is the frequency value corresponding to a complete bilayer and equals −26 Hz, as reported in past studies (*8*). As the average vesicle diameter increases, incomplete bilayer formation is demonstrated by a decrease in the rupturing percentage from 99% to 12%. For vesicles with an average diameter greater than 250 nm, the rupturing percentage is not a useful calculation because AH peptide's interaction with these larger vesicles is insufficient to cause a structural transformation. Instead, we calculated the AH peptide binding mass (Figure 3, panel f) by using the Sauerbrey relationship, which relates the frequency change to the mass change, to demonstrate that AH peptide binding is the predominant interaction for larger vesicles.

These results suggest that vesicles must possess a maximum line tension, as demonstrated by the vesicle size dependency, in order for AH peptides to cause vesicle rup-

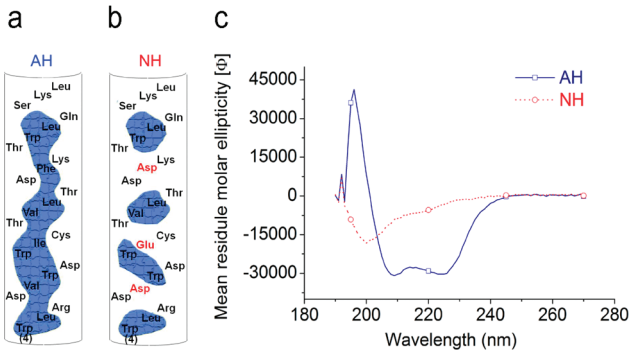

Figure 1. Helix net diagrams and circular dichroism measurements of AH and NH Peptides. a) The amphipathic, α-helical (AH) peptide derived from the N-terminus of HCV NS5A is depicted in a helix net diagram, wherein the cylindrical α-helical segment is "cut" along one face and then "flattened" into the plane of the page. The amino acid sequence of NS5A from amino acids 4 to 27 in the N-terminal to C-terminal direction is shown with the long continuous stretch of hydrophobicity indicated in blue. b) A nonamphipathic, nonhelical (NH) peptide was also designed by substitution of three charged amino acids into the AH peptide at the indicated positions, such that no sustained hydrophobic patch remained (*2*). c) Circular dichroism spectra of AH and NH peptides. The blue spectrum is the AH peptide demonstrating its α-helical character, and the red spectrum corresponds to the NH peptide, which no longer displays any significant helical structure.

ture and subsequent bilayer formation (*5, 9*). Using a combined QCM-D and reflectometry setup, we recently compared the vesicle rupturing process on two different substrates, gold and silica. While the vesicle−vesicle and vesicle−substrate interactions are sufficient to cause vesicle rupture on a silica substrate, AH peptide's interaction with the adsorbed vesicles is necessary, in addition to these other interactions, to cause vesicle rupture on a gold substrate. AH peptide binds to the vesicle surface, promotes vesicle swelling, and then desorbs. In comparison to the vesicle rupturing process on silica, the AH peptide-catalyzed process is nearly identical on gold, despite the different, initial vesicle adsorption process.

In our model system, as the vesicle is attracted toward the gold substrate, which has a highly polarized state, the adhesion and bending energies increase (*8*). The adhesion energy dominates the rupturing process because the bending energy change is independent of vesicle size. Further, an AFM study supports the adhesion energy's importance by demonstrating that adsorbed vesicles retain a certain height−width ratio (*10*). However, the adhesion energy is not sufficient to cause vesicle rupture on the gold substrate. For small vesicles with a maximum membrane tension, the AH peptide binding interaction destabilizes the vesicle structure to such an extent that the energy barrier for vesicle rupture is overcome. We hypothesize that the reduced or nonexistent rupturing of larger vesicles upon AH peptide binding is due to the vesicles possessing an insufficient line tension that is related to their reduced vesicle curvature. The local morphology of these larger vesicles is more similar to that of a planar bilayer, to which we have previously demonstrated that the AH peptide's interaction is limited to binding (*3*). With that observation, taken together with the QCM-D results of this study, the vesicle size dependence of AH peptide's vesicle rupturing ability appears to be related to morphological differences of the target vesicles, though the interaction with the substrate on which the vesicles are absorbed may also influence this relationship (*11*). In the case of employing the AH peptide as an antiviral agent, the diameter range over which the AH peptide can catalyze vesicle rupture includes a wide range of medically important viruses.

Based on the AH peptide's interaction with vesicles serving as models of virus particles, we hypothesized that AH peptide treatment might have similar disruptive effects on the lipid envelopes of a variety of medically important viruses within the size range determined to be susceptible to vesicle lysis. To test this hypothesis, we treated an inoculum of HCV (average particle diameter of 50 nm (*12*), produced in tissue culture as described elsewhere (*13*)), with either AH or control NH peptides. We used AFM to examine the physical effect of AH peptides on HCV particles. AFM analysis revealed a significant decrease in the number of apparently intact virus particles upon AH, but not NH, peptide treatment (Figure 4, panels a−c). Images of intact virus particles by themselves (Figure 4, panel a) and treated with NH peptide

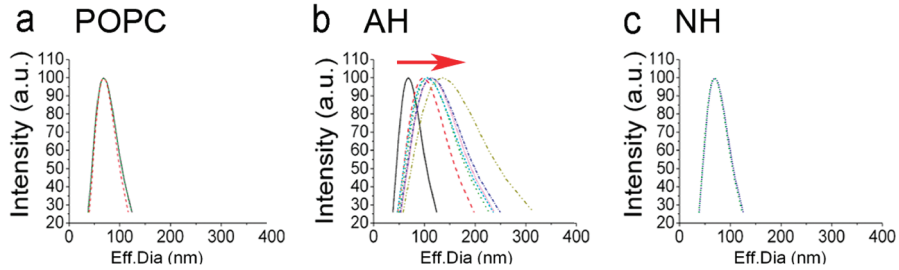

Figure 2. Dynamic light scattering (DLS) monitoring of vesicle interactions with AH and NH peptides. a) Intensity-weighted size distribution of POPC vesicles without peptide as measured by DLS. Multiple scans performed over 1 h are shown with no change in size distribution. b) The average effective diameter increased due to membrane disruption and reassembly of POPC vesicles following AH peptide treatment. Red bar indicates increasing time. c) No changes are observed following NH peptide treatment.

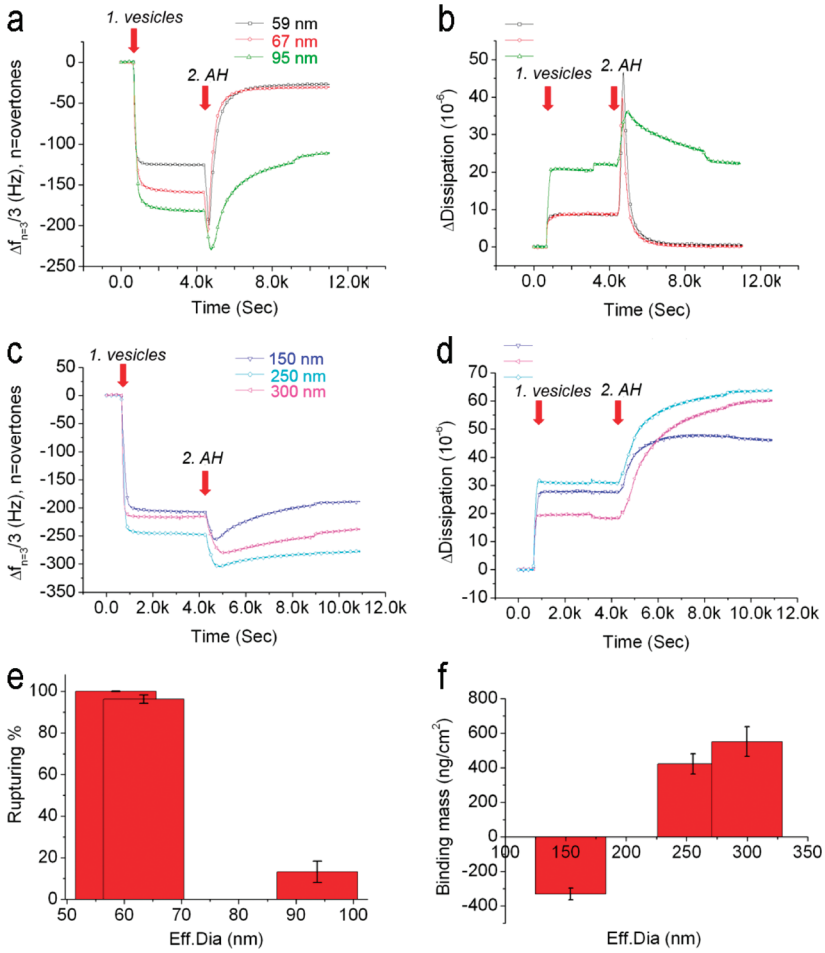

Figure 3. Antiviral mode of action of the AH peptide assayed using a biomimetic, self-assembly based QCM-D platform. a) QCM-D frequency response for various vesicle size distributions up to 100 nm upon AH peptide addition (vesicles added at first arrow at 1.0 ks; AH peptide added at second arrow at 4.2 ks). b) Corresponding energy dissipation changes. c) QCM-D frequency response for vesicle size distributions greater than 100 nm upon AH peptide addition. d) Corresponding energy dissipation changes. Note that the graphs below present the average vesicle effective diameters as measured by DLS. e) Calculation of rupturing efficiency from the frequency response (Supplementary Figure 1), as a function of vesicle size. One hundred percent rupturing is defined as complete rupturing of adsorbed lipid vesicles with subsequent formation of a complete lipid bilayer having the characteristic frequency change of ~26 Hz (*8*). f) The absolute bound mass change is determined by using the Sauerbrey equation, in which frequency change is linearly proportional to mass change, calculated using the data from Figure 3, panels a and b.

(Figure 4, panel c) were compared with ruptured virus particles due to AH peptide treatment (Figure 4, panel b).

On the basis of the decrease in the number of apparently intact HCV particles upon AH peptide addition, the treatment is expected to also result in a decrease in HCV's infection potential. Infectivity assays support this prediction, namely, that treatment with AH peptide dramatically reduced the infectivity of HCV particles (Figure 5, panel a and Supplementary Figure S2). In contrast, analogous experiments performed with vaccinia virus (average particle diameter of 360 nm (*14*)) indicates that AH peptide does not significantly decrease this virus' infection potential (Figure 5, panel a). Similar results have recently been reported by Cheng et al. (*15*), where a larger number of viruses were treated with AH peptide, although no mechanism was provided to account for the varying effects of the AH peptide on the various viruses. Our results, however, now offer an attractive and experimentally verified explanation for the seemingly unpredictable sensitivities of a given virus to AH peptide treatment.

Indeed, as shown in Figure 5, panel b, a good correlation, albeit with some caveats discussed below, exists between virus particle size and AH peptide lysis potency, with the latter most effective for smaller diameter viruses. Using data presented in ref 15, viruses with various size distributions of particles were plotted as a function of average particle diameter. Susceptibility to peptide-mediated inhibition of infectivity was determined on the basis of the antiviral activity of an 18 amino acid fragment of the AH peptide used in this study, termed C5A (*15*). On the basis of the size cutoff below which 100% lipid vesicle rupture by AH peptide occurred (green dotted line), as determined by QCM-D experiments, we propose that our lipid vesicle model represents a reliable model system for predicting AH peptide sensitivity of individual viruses when the latter best approximate the lipid vesicles used in our studies that (i) have a lipid envelope, (ii) have a relatively uniform size distribution, and (iii) have minimal heterogeneity in physical particle shape. Of note, several of the viruses indicated in Figure 5, panel a do not conform to one or more of these criteria. Removing such viruses results in an even stronger correlation between virus particle size and sensitivity to AH peptide.

Note that the threshold for AH peptide-mediated lysis indicated in Figure 5, panel a essentially corresponds to the necessary

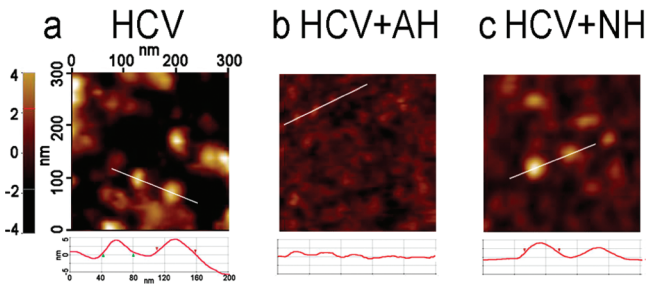

Figure 4. Atomic force microscopy (AFM) imaging of AH peptide's interaction with HCV virus particles. HCV virus particles on mica (a) are ruptured after addition of AH peptide (b) but remain intact after NH peptide treatment (c).

vesicle diameter range for complete rupturing as measured by the QCM-D experiments. However, as demonstrated by the QCM-D results that indicate vesicle rupturing for larger vesicles is reduced but not altogether absent, it is likely that the AH peptide's virus particle lysis occurs on a continuum. While smaller diameter virus particles are more efficiently lysed, some larger sized particles may still be affected by the AH peptide. Therefore, larger sized virus particles may still be partially impaired in appropriate infectivity assays. While size dependency may be a significant factor in determining whether AH peptide is virocidal against a specific virus, this does not rule out that there are other important factors. For example, our previous study demonstrated that association of AH peptide on model membranes can be greatly enhanced by proteinaceous components (*3*). Cheng and co-workers reported that an 18 amino acid peptide derived from the N-terminal AH region of NS5A has virocidal activity against the Dengue virus and HIV, both of which possess cellular components similar to HCV virus membranes, suggesting that lipid composition may have a certain role in the lysis effect (*15, 16*). Further, our recent work suggests that the initial AH peptide–vesicle interaction promotes swelling of the vesicles, which leads to vesicle lysis (*11*). AH peptide's potency may also be affected by parameters such as the electrostatic interaction (*e.g.*, lipid composition of the vesicles) and membrane rigidity (*e.g.*, cholesterol and sphingolipid content), among other possibilities.

In conclusion, the above results provide new insights into an unanticipated property of a virally encoded AH peptide. In addition to previously reported roles in mediating membrane association (*3*), viral membrane-associated RNA genome replication (*2*), and interaction with key regulators of intracellular membrane vesicle trafficking machinery (*13*), our results reveal that when present in an isolated, non-natural context, the AH peptide of HCV NS5A is a potent mediator of lipid vesicle and lipid membrane-bound virus particle lysis. The efficiency of this activity exhibits a size dependence that falls within the range of a wide array of medically important viruses.

Although it is not clear how this activity might be employed by HCV during its life cycle, this activity can now be exploited for a variety of practical purposes. In particular, AH peptide-mediated vesicle rupture represents a biochemical activity that may both serve as a convenient assay for inhibitors designed to disrupt AH function, as well as a practical treatment aimed at disrupting

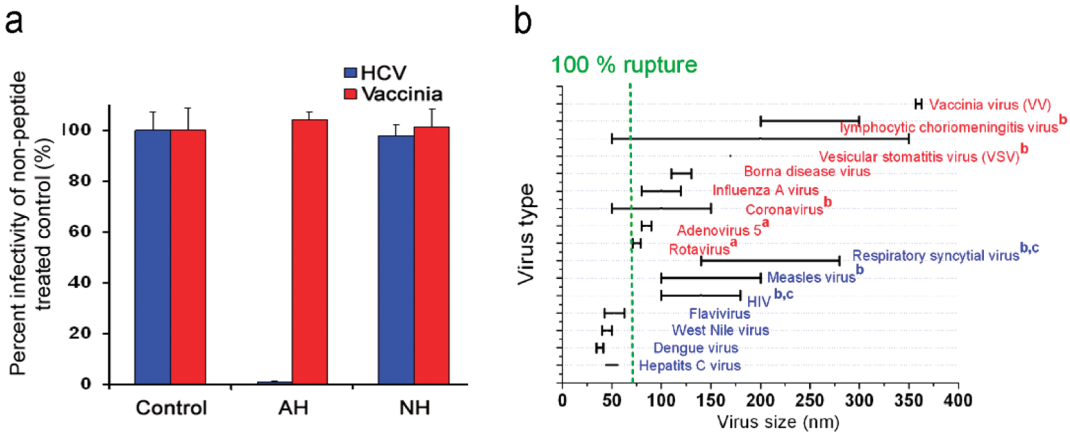

Figure 5. Virus lysis potential of AH peptide. a) Infectivity assays demonstrating AH peptide-mediated disruption of virus particles for small (HCV) but not large (vaccinia) viruses. Inoculums of HCV (~50 nm particle diameter) and vaccinia virus (~360 nm) were treated with either AH or NH peptides, and the infectivity of the treated inoculums was determined and expressed as a percentage of nonpeptide treated control (see Supporting Information). b) The graph represents data replotted from ref 15, wherein the size distribution of the viruses is indicated by the black bars. Susceptibility to AH peptide-mediated inhibition of infectivity is indicated for a variety of viruses, as determined in ref 15. Viruses reported to be susceptible and refractory to AH-mediated treatment are indicated in blue and red, respectively. Size cutoff below which 100% lipid vesicle rupture occurs is indicated by the vertical green dotted line. Viruses that (i) do not have a lipid envelope, (ii) do not have a relatively uniform size distribution, or (iii) have heterogeneity in physical particle shapes are indicated with the corresponding superscript letters, a, b, and c, respectively.

lipid membrane-bound virus particles. Moreover, the experimental methods we have used incorporate model platforms whose properties can be modified to further study the molecular determinants of AH peptide-mediated vesicle and virus particle lysis. Finally, in the case of HCV, our results suggest that the NS5A AH peptide might be used to rupture viruses extra-corporally (for HCV prevention) and within infected individuals (for HCV therapy).

METHODS

Dynamic Light Scattering. DLS was performed using a doubled, Nd:YAG laser (model 532 DPSS, Coherent Laser Group, Santa Clara, CA) with a wavelength, λ, of 633 nm with a Brookhaven digital autocorrelator and analyzed by digital autocorrelator software (Brookhaven Instruments Corporation, New York, NY). Measurements of the intensity autocorrelation function were performed at a scattering angle of 90° using a linear spacing of the correlation time. DLS results were analyzed to give an intensity-weighted size distribution using a discrete Laplace inversion routine. All measurements were taken at a scattering angle of 90° where the reflection effect is minimized. All autocorrelation functions were also analyzed by CONTIN and nonnegatively constrained least squares (NNLS) algorithms to check for multimodal distributions.

Quartz Crystal Microbalance-Dissipation. Adsorption kinetics and the properties of the adsorbed layer were studied using a Q-Sense E4 four chamber system (Q-Sense AB, Gothenburg, Sweden). The samples are introduced using a peristaltic pump with flow rate of 0.1 mL·min^{-1}. AT-cut gold crystals (Q-Sense) of 14 mm in diameter with a 50 nm thick gold-coated sensor surface were used for all vesicle interaction and adsorption experiments. Each QCM crystal was treated with oxygen plasma at ~80 W for ~3 min prior to measurements (March Plasmod Plasma Etcher, March Instruments, Concord, CA). The crystal was initially driven near its resonance frequency as indicated by a maximum in the current. To capture the characteristic dissipation, the drive circuit was short-circuited and the exponential decay of the crystal oscillation was recorded and analyzed, yielding the frequency and dissipation changes at 5, 15, 25, 35, 45, 55, and 65 MHz, respectively. The temperature of the Q-Sense cell was set at 25.0 °C and accurately controlled by a Peltier element in the cell with fluctuations smaller than ±0.05 °C. All experiments were repeated at least three times, with a standard deviation of less than 1%.

Atomic Force Microscopy. The AFM experiments were carried out on a XE-Bio (Park Systems, Suwon, Korea) in contact and noncontact modes. Rectangular-shaped silicon cantilevers were used (SICON for contact mode and ACT for noncontact mode, AppNano, Santa Clara, CA). The cantilevers had a force constant of $k = 0.1$ N/m for SICON and 25 N/m for ACT and average tip radius of 5−6 nm. All measurements were performed in a Tris buffer. Images of virus were obtained both in the "contact" mode with an imaging force of less than 200 pN and with "non-contact" mode in fluid. However, images presented in this manuscript were only obtained in the "non-contact" mode in fluid. The scan line speed was optimized between 0.3 and 1 Hz with a pixel number of 256 × 256, depending on the scan size. Images were recorded in height, amplitude, phase, and error modes. All measurements were done on the height images. All images shown were subjected to a first-order plane-fitting procedure to compensate for sample tilt. The cross-sectional analysis was carried out on images subjected only to a first order plane-fitting procedure. Topographical and grain analyses of virus preparations were performed using the software XEI 1.7.1 supplied by Park Systems.

Circular Dichroism. CD measurements were carried out using an Aviv Model 215 equipped with a 450 W xenon arc lamp light source. CD scans in wavelength mode were recorded in the range of 190−270 nm at 1.0 nm steps and averaged over two scans with averaging time = 5.0 s per datum point. Measurements were carried out at 25 °C. Spectral units were expressed as the molar ellipticity per residue by using peptide concentrations determined by measuring the UV light absorbance of tyrosine and tryptophan at 280 nm. The secondary scans were corrected for background based on blanks of Tris buffer. The scans obtained with ellipticity (Θ) were converted to mean molar residue ellipticity ([Θ]) as previously described (*17*). Spectra were processed with CD6 software, baseline-corrected, and smoothed using a third-order least-squares polynomial fit.

Small Unilamellar Vesicle Preparation. Vesicles of 1-palmitoyl-2-oleoyl-sn-glycero-3-phosphocholine (POPC) (Avanti Polar Lipids, Alabaster, AL) with different size distributions were prepared by the combination of freeze−thaw cycles and the extrusion method. The model system was selected on the basis of the following consideration. Self-assembly monolayer (either intact vesicle or supported lipid bilayer on gold) was composed of a single POPC lipid that has a fluid−solid phase transition temperature (~ −10 °C) well below the experimental temperature of 24 °C. Throughout the experiments, we used a Tris buffer (10 mM Tris-HCl, pH 7.5 and 150 mM NaCl) in 18.2 MΩ-cm Milli-Q water (MilliPore, Oregon). Extruded vesicles (referred to simply as vesicles) were prepared in the following manner. Lipid films were prepared by first drying the as-supplied lipids dissolved in chloroform under a gentle stream of nitrogen at RT. Then the resulting lipid film was stored under vacuum for at least 5 h in order to remove residual chloroform. Vesicles were first prepared by swelling the dried lipid film in an aqueous solution, followed by vortexing periodically for 5 min. Further, in order to effectively get rid of vesicle multilamellarity, we used seven cycles of the freeze−thaw technique. We first froze the vesicle sample with liquid nitrogen, then thawed it in a 60 °C water bath following by vortexing. The resulting vesicle solutions were subsequently sized by a mini extruder (Avanti Polar Lipids) through polycarbonate membranes with nominal sizes of 1000-, 400-, 200-,100-, 50-, and 30-nm pores. Vesicles were generally prepared at a nominal lipid concentration of ~5 mg mL^{-1} and then subsequently diluted before experiments. Vesicles were generally used within a day of preparation.

Peptides. Amphipathic α-helical peptides (AH) and nonamphipathic nonhelical peptides (NH) were synthesized by Anaspec Corporation (San Jose, CA). Whereas the AH peptide is helical with an extended hydrophobic domain (blue in Figure 1), NH peptides were designed to introduce three charged amino acids (red in Figure 1) so as to disrupt the hydrophobic face of the AH peptide. The sequences of AH and NH peptides are H-Ser-Gly-Ser-Trp-Leu-Arg-Asp-Val-Trp-Asp-Trp-Ile-Cys-Thr-Val-Leu-Thr-Asp-Phe-Lys-Thr-Trp-Leu-Gln-Ser-Lys-Leu-NH_2 and H-Ser-Gly-Ser-Trp-Leu-Arg-Asp-**Asp**-Trp-Asp-Trp-**Glu**-Cys-Thr-Val-Leu-Thr-Asp-**Asp**-Lys-Thr-Trp-Leu-Gln-Ser-Lys-Leu-NH_2, respectively (the introduced charged amino acids are indicated in bold underline).

Infectivity Assays. Infectious viral stocks of HCV and vaccinia virus were prepared as described previously (*2, 13*). Peptides were reconstituted in water at a concentration of 0.26 mM and stored at −80 °C. Peptides were diluted in serum-free medium containing 1.2×10^4 focus-forming units (FFU) mL^{-1} of HCV or 85 plaque-forming units (PFU) mL^{-1} of vaccinia virus to a final concentration of 13 μM and incubated at RT for 0.5 h. The virus-peptide mixtures were then used to infect Huh 7.5 cells in a 96-well plate for HCV or CV1 cells in 6-well plates for vaccinia virus. After adsorption for 2 h at 37 °C, the inocula were removed, and fresh growth medium was added to the cells for 3 days. Huh7.5 cells were then fixed with 4% formaldehyde and immunostained with primary antibody against the HCV structural core protein (*18*) and secondary antibody conjugated to Alexa 594. The numbers of HCV-positive foci were counted by fluorescence microscopy. Vaccinia virus plaques were counted following cell fixation and staining with crystal violet. Results are expressed as a percentage of the infectivity associated with the non-peptide-treated control inoculum.

Acknowledgment: This work was supported by a Burroughs Welcome Fund Clinical Scientist Award in Translational Research (to J.S.G.), and RO1-DK064223. N.J.C. is a recipient of an American Liver Foundation Postdoctoral Fellowship Award, a Global Roche Postdoctoral Fellowship, and a Stanford Dean's Postdoctoral Fellowship.

Supporting Information Available: This material is available free of charge *via* the Internet at http://pubs.acs.org.

REFERENCES

1. Moradpour, D., Penin, F., and Rice, C. M. (2007) Replication of hepatitis C virus, *Nat. Rev. Microbiol. 5*, 453−463.

2. Elazar, M., Cheong, K. H., Liu, P., Greenberg, H. B., Rice, C. M., and Glenn, J. S. (2003) Amphipathic helix-dependent localization of NS5A mediates hepatitis C virus RNA replication, *J. Virol. 77*, 6055–6061.
3. Cho, N. J., Cheong, K. H., Lee, C., Frank, C. W., and Glenn, J. S. (2007) Binding dynamics of hepatitis C virus' NS5A amphipathic peptide to cell and model membranes, *J. Virol. 81*, 6682–6689.
4. Cho, N. J., Kanazawa, K. K., Glenn, J. S., and Frank, C. W. (2007) Employing two different quartz crystal microbalance models to study changes in viscoelastic behavior upon transformation of lipid vesicles to a bilayer on a gold surface, *Anal. Chem. 79*, 7027–7035.
5. Cho, N. J., Cho, S. J., Cheong, K. H., Glenn, J. S., and Frank, C. W. (2007) Employing an amphipathic viral peptide to create a lipid bilayer on Au and TiO_2, *J. Am. Chem. Soc. 129*, 10050–10051.
6. Rodahl, M., Hook, F., Fredriksson, C., Keller, C. A., Krozer, A., Brzezinski, P., Voinova, M., and Kasemo, B. (1997) Simultaneous frequency and dissipation factor QCM measurements of biomolecular adsorption and cell adhesion, *Faraday Discuss.* 229–246.
7. Sauerbrey, G. (1959) Verwendung Von Schwingquarzen Zur Wagung Dunner Schichten Und Zur Mikrowagung, *Z. Phys 155*, 206–222.
8. Keller, C. A., and Kasemo, B. (1998) Surface specific kinetics of lipid vesicle adsorption measured with a quartz crystal microbalance, *Biophys. J. 75*, 1397–1402.
9. Seifert, U., Berndl, K., and Lipowsky, R. (1991) Shape transformations of vesicles—phase-diagram for spontaneous-curvature and bilayer-coupling models, *Phys. Rev. A 44*, 1182–1202.
10. Schonherr, H., Johnson, J. M., Lenz, P., Frank, C. W., and Boxer, S. G. (2004) Vesicle adsorption and lipid bilayer formation on glass studied by atomic force microscopy, *Langmuir 20*, 11600–11606.
11. Cho, N. J., Wang, G. L., Edvardsson, M., Glenn, J. S., Hook, F., and Frank, C. W. (2009) α-Helical peptide-induced vesicle rupture revealing new insight into the vesicle fusion process as monitored in situ by quartz crystal microbalance-dissipation and reflectometry, *Anal. Chem. 81*, 4752–4761.
12. Yu, X., Qiao, M., Atanasov, I., Hu, Z., Kato, T., Liang, T. J., and Zhou, Z. H. (2007) Cryo-electron microscopy and three-dimensional reconstructions of hepatitis C virus particles, *Virology 367*, 126–134.
13. Sklan, E. H., Staschke, K., Oakes, T. M., Elazar, M., Winters, M., Aroeti, B., Danieli, T., and Glenn, J. S. (2007) A Rab-GAP TBC domain protein binds hepatitis C virus NS5A and mediates viral replication, *J. Virol. 81*, 11096–11105.
14. Cabezas, P., and Risco, C. (2006) Studying cellular architecture in three dimensions with improved resolution: Ta replicas revisited, *Cell Biol. Int. 30*, 747–754.
15. Cheng, G., Montero, A., Gastaminza, P., Whitten-Bauer, C., Wieland, S. F., Isogawa, M., Fredericksen, B., Selvarajah, S., Gallay, P. A., Ghadiri, M. R., and Chisari, F. V. (2008) A virocidal amphipathic α-helical peptide that inhibits hepatitis C virus infection *in vitro*, *Proc. Natl. Acad. Sci. U.S.A. 105*, 3088–3093.
16. Bobardt, M. D., Cheng, G., de Witte, L., Selvarajah, S., Chatterji, U., Sanders-Beer, B. E., Geijtenbeek, T. B., Chisari, F. V., and Gallay, P. A. (2008) Hepatitis C virus NS5A anchor peptide disrupts human immunodeficiency virus, *Proc. Natl. Acad. Sci. U.S.A. 105*, 5525–5530.
17. De Marco, V., De Marco, A., Goldie, K. N., Correia, J. J., and Hoenger, A. (2003) Dimerization properties of a *Xenopus laevis* kinesin-II carboxy-terminal stalk fragment, *EMBO Rep. 4*, 717–722.
18. Matto, M., Rice, C. M., Aroeti, B., and Glenn, J. S. (2004) Hepatitis C virus core protein associates with detergent-resistant membranes distinct from classical plasma membrane rafts, *J. Virol. 78*, 12047–12053.